



On-Chip Strong Coupling and Efficient Frequency Conversion between Telecom and Visible Optical Modes

Xiang Guo, Chang-Ling Zou, Hojoong Jung, and Hong X. Tang*

Department of Electrical Engineering, Yale University, New Haven, Connecticut 06511, USA

(Received 28 January 2016; published 16 September 2016)

While the frequency conversion of photons has been realized with various approaches, the realization of strong coupling between optical modes of different colors has never been reported. Here, we present an experimental demonstration of strong coupling between telecom (1550 nm) and visible (775 nm) optical modes on an aluminum nitride photonic chip. The nonreciprocal normal-mode splitting is demonstrated as a result of the coherent interference between photons with different colors. Furthermore, a wideband, bidirectional frequency conversion with 0.14 on-chip conversion efficiency and a bandwidth up to 1.2 GHz is demonstrated.

DOI: [10.1103/PhysRevLett.117.123902](https://doi.org/10.1103/PhysRevLett.117.123902)

Developments in classical and quantum information technologies have spurred the study of photonics, attributed to the photon's long coherence time, low transmission loss, and high speed. Coherent coupling between photons with various matter qubit systems such as atomic ensembles [1] and quantum dots [2] has been realized. These systems, however, favor photons of visible or near infrared wavelength, which are not suitable for long distance communication through fiber. As a result, coherent frequency conversion between visible and telecom bands is of great interest and has been realized with different methods, including three wave mixing ($\chi^{(2)}$ nonlinearity) [3–6], four wave mixing ($\chi^{(3)}$ nonlinearity) [7–9], and optomechanical interactions [10,11]. Among them, the implementations of frequency conversion with integrated photonic devices [12,13] are of special interest due to device's small footprints and scalability [14,15]. In addition, owing to the high quality factor to mode volume ratio, microcavity based devices are promising for enhanced photon-photon interactions.

In this Letter, we demonstrate the strong coupling between optical modes of different colors on a scalable aluminum nitride-on-insulator [16] chip, bringing the cavity nonlinear optics into a new regime, and also offering a unique way to realize all-optical control, isolation, and efficient frequency conversion. Under the parametric pumping of an optical drive field, normal-mode splitting [1,17] is observed, which is the benchmark for coherent coupling between the visible mode and the telecom mode. Because of the inherent phase matching condition in the traveling wave cavity, the demonstrated coherent interaction and the accompanying mode splitting are nonreciprocal [18,19], which permits future applications such as nonmagnetic, ultrafast optical isolators [20–22]. We further realize bidirectional optical frequency conversion between the telecom band and visible band with 0.14 on-chip (photon flux) conversion efficiency. The demonstrated strong coupling between photons of different colors is of

fundamental interest for quantum optics and provides a kernel device for the realization of a quantum internet [23].

Figure 1(a) illustrates the fabricated aluminum nitride (AlN) microring structure. The $\chi^{(2)}$ nonlinearity of the AlN microring induces the interaction between three modes of different colors. We choose transverse-magnetic (TM) modes because the TM mode has higher $\chi^{(2)}$ nonlinearity as compared to transverse-electric (TE) modes in our AlN chip. To fulfill the required phase match condition of three-wave mixing process, we engineer the width of the microring [24,25] to match the refractive index of the fundamental TM (TM₀) mode in the telecom band to the refractive index of the third order TM (TM₂) mode in the visible band. Their respective mode profiles are shown in the insets of Fig. 1(a). Because dual wavelength bands are involved in this system, we design two bus waveguides to couple with the telecom TM₀ mode and visible TM₂ mode separately [Fig. 1(a)]. In the following we adopt a quantum optics description of our system, although a classical description is also viable. The three wave mixing in the microring can be described by the Hamiltonian

$$\mathcal{H} = \omega_{a0}\hat{a}^\dagger\hat{a} + \omega_{b0}\hat{b}^\dagger\hat{b} + \omega_{c0}\hat{c}^\dagger\hat{c} + g(\hat{a}\hat{b}^\dagger\hat{c} + \hat{a}^\dagger\hat{b}\hat{c}^\dagger). \quad (1)$$

Here, \hat{a} , \hat{b} , and \hat{c} are the bosonic operators for three TM modes in the microring. g is the nonlinear single-photon interaction strength and is dependent on the $\chi^{(2)}$ coefficient of the material, field overlap for three modes, as well as mode volumes [26]. Additionally, the momentum conservation condition ($m_a + m_c = m_b$) must be fulfilled for a nonvanishing g , which demands all three modes traveling in the same direction in the microring resonator to get involved in the nonlinear interaction process. This directionality further results in a nonreciprocal transmission spectrum for the probe mode's resonance. In the experiment, we choose modes a , c in the telecom band and mode b in the visible band. The measured transmission spectra of the

modes and the schematic diagram of their frequencies are depicted in Fig. 1(b). Here, telecom modes a and c are almost critically coupled [30] [$\kappa_{a,1}(\kappa_{c,1}) = \kappa_{a,0}(\kappa_{c,0})$, where $\kappa_{x,0}(\kappa_{x,1})$ is the intrinsic (external) loss rate of mode x], while visible mode b is slightly undercoupled ($\kappa_{b,1} < \kappa_{b,0}$). The loaded quality factors and linewidth for modes a , b , and c are $Q_{\text{load},a}(Q_{\text{load},b}, Q_{\text{load},c}) = 1.8 \times 10^5(1.1 \times 10^5, 2.6 \times 10^5)$ and 1.08 (3.53, 0.74 GHz), respectively.

As we aim for the coherent coupling between the telecom and visible photons, we strongly drive mode a by a near resonance strong laser (ω_a) and hence stimulate large exchange coupling strength between mode b and c . The simplified system Hamiltonian reads [26]

$$\mathcal{H} = \omega_{b0}\hat{b}^\dagger\hat{b} + \omega_{c0}\hat{c}^\dagger\hat{c} + G\hat{c}\hat{b}^\dagger e^{-i\omega_a t} + G^*\hat{c}^\dagger\hat{b}e^{i\omega_a t}, \quad (2)$$

where $G = \langle \hat{a} \rangle g$ is the effective interaction strength, with $|\langle \hat{a} \rangle|^2 \propto P_a$ the mean photon number of mode a and P_a is the power of the drive laser. This beam-splitter-like Hamiltonian indicates that photons in cavities b and c can be converted to each other coherently without introducing additional noises [3], just like a linear optics device.

It is instructive to introduce a simplified model, as depicted in Fig. 1(c), where two resonators loaded by two separate bus waveguides are used to represent the resonant modes b and c separately. We model the effective interaction strength G as a controllable coupling switch between the two optical modes with different colors. If there is no driving ($G = 0$), the two resonators are

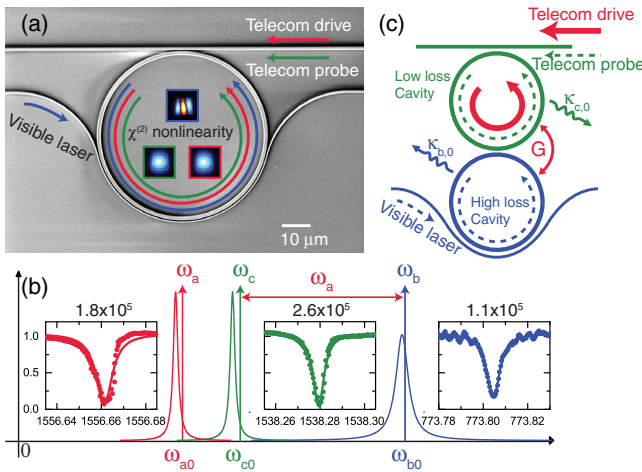


FIG. 1. Triply resonant microring resonator coupled by second order optical nonlinearity. (a) SEM picture of the core device. Three optical modes coexist in the microring resonator, and couple through $\chi^{(2)}$ nonlinear interaction. Insets are the field distributions of the cross section. (b) Schematics of the optical modes' frequencies and their respective transmission spectrum. (c) Coupled resonator model for the coherent interaction in a $\chi^{(2)}$ microring resonator. Here the coupling between the telecom and visible probe modes is controlled by the telecom drive laser.

decoupled from each other and photons cannot tunnel from one ring to the other (physically, this means photons cannot change color without nonlinear interaction). When the drive laser is on and nonlinear interaction G is nonzero, the two ring cavities start to couple together and photons in one resonator can couple into the other one (physically, it means that photons' colors get changed due to nonlinear interaction) and even coupled back when the G is comparable to the cavities' loss rates. Note that this nonlinear interaction process is nonreciprocal because G vanishes for the probe lights propagating in the opposite direction of the drive laser due to momentum mismatch [26].

From the schematic illustrated by Fig. 1(c), the most straightforward outcome of the coherent coupling between two coupled resonators is the modified resonance spectrum. We can also see this via the energy diagram [26], where two pathways are connected to the same energy level and induce interference [31]. Physically, when visible photons enter the microring, they can be coherently scattered into telecom photons by the strong drive laser. The generated telecom photons can be converted back to visible photons and result in destructive interference for the probe laser. When the coupling strength G is comparable or even larger than the resonators' dissipation rates, the coherent conversion beats the decoherence and normal-mode splitting emerges. Using the experimental setup shown in Fig. 2(a), the transmission spectrum of the visible mode is probed. The telecom drive laser (ω_a , near the resonant frequency ω_{a0} of mode a) excites the counterclockwise (CCW) propagating mode in the microring, while a visible laser (ω_b) probes the transmission of mode b (centered at ω_{b0}) in either the clockwise (CW) or CCW direction. Figure 2(b) plots the spectra of mode b probed from different directions with drive laser fixed. A mode splitting spectrum is observed when the visible laser propagates in the same direction (CCW) as the drive laser. In contrast, when the probe laser propagates in the counter-propagating direction (CW) of the drive laser, the resonance is of normal Lorentzian shape, similar to the transmission spectrum without parametric pumping [Fig. 2(c), top panel]. The comparison of the spectra for two propagating directions clearly reveals the nonreciprocal nonlinear effect in the microring.

The observed mode splitting is further tested with different powers of the drive laser [Fig. 2(c)]. A clearly increased splitting level is observed with the increase of launched drive laser power. Following the Hamiltonian [Eq. (2)] and considering the linear losses of modes b and c , we derive the theoretical formula for the transmission of the visible mode b as

$$T = \left| 1 + \frac{2\kappa_{b,1}}{-i\delta_b - \kappa_b + \frac{|G|^2}{-i\delta_c - \kappa_c}} \right|^2, \quad (3)$$

where $\kappa_{a(b)} = \kappa_{a(b),0} + \kappa_{a(b),1}$ is the total loss rate, $\delta_b = \omega_{b0} - \omega_b$ and $\delta_c = \omega_{c0} - (\omega_b - \omega_a)$ are the angular

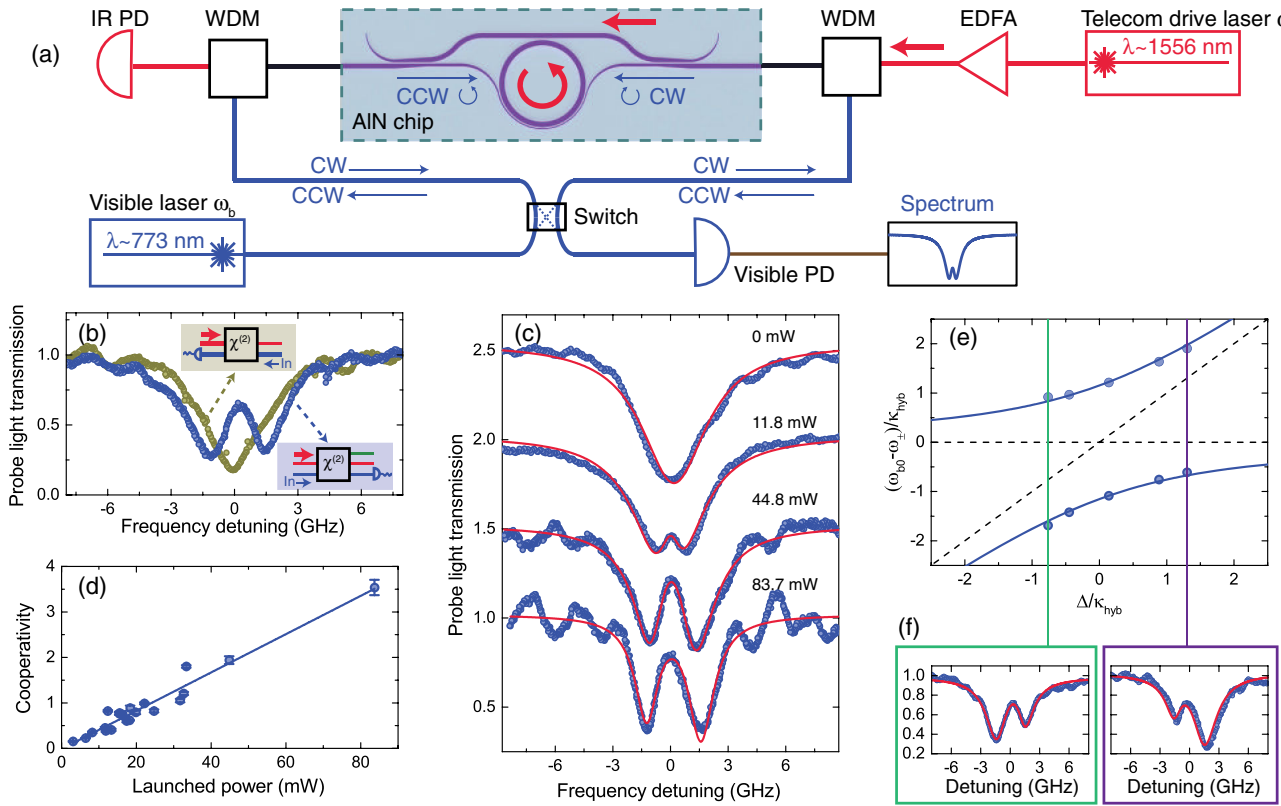


FIG. 2. Strong coupling due to $\chi^{(2)}$ nonlinear interaction. (a) Experimental setup. Telecom laser ω_a strongly excites mode a in the microring resonator with CCW propagation direction. A visible probe laser ω_b is used to probe the transmission spectrum of mode b (centered at ω_{b0}) from either the CW or CCW direction. (b) Transmission spectra of mode b with either CW or CCW directions. The data are plotted in linear scale. In both insets, the giant red arrow represents the input direction of the telecom drive laser while the blue arrow represents the input direction of the visible probe laser. The red solid lines are fittings with Eq. (3). The transmission in the center of the resonance increases from 27% (with 0 mW drive power) to 80% (with 83.7 mW drive power) of the total transmission. The data is shown in linear scale, and the vertical axes of the four transmission curves have been offset for clarity. (d) Extracted cooperativities at different drive powers. (e) Frequencies of dressed modes (ω_{\pm}) under different values of Δ . The solid line is the theoretical fitting curve. (f) Fano-like transmission spectra when $\Delta \neq 0$.

frequency detunings of mode b and c , respectively. The experimental results are fitted according to Eq. (3) and exhibit valid agreements, as shown by the red solid lines in Fig. 2(c). Here $\kappa_{b(c)}$, $\kappa_{b,1}$, G and $\Delta = \delta_c - \delta_b = \omega_a + \omega_{c0} - \omega_{b0}$ are treated as fitting parameters. Cooperativity $C = |G|^2/\kappa_b\kappa_c$ [10,11,19,31] is usually used in hybrid systems as a figure-of-merit to evaluate the coherent coupling between two different modes. It is closely related to the concept of strong coupling, where the coupling strength is bigger than the loss rates of both modes ($|G| > \kappa_b, \kappa_c$). To quantify the coherent interaction strength, the cooperativity C is extracted from each transmission spectrum and plotted against drive laser power P_a [Fig. 2(d)]. The linear dependence of C over the launched drive power is observed, as expected by theory that $C \propto |G|^2 \propto P_a$. From the data in Fig. 2(d), a unit power cooperativity of $C/P_a = 0.042 \pm 0.001 \text{ mW}^{-1}$ is derived. Specifically, with the highest power we applied (83.7 mW), a maximum cooperativity of 3.53 is achieved with $|G| = 2\pi \times 1.38$, $\kappa_b = 2\pi \times 1.00$, and $\kappa_c = 2\pi \times 0.54 \text{ GHz}$. The strong coupling ($|G| > \kappa_b, \kappa_c$)

is clearly observed from the bottom-most curve in Fig. 2(c), which indicates that the telecom and visible modes are coherently coupled and hybridized into two dressed states, whose frequencies read

$$\omega_{\pm} = \omega_{b0} + \frac{1}{2}\Delta \pm \frac{1}{2}\sqrt{4G^2 + \Delta^2}. \quad (4)$$

The extracted values of ω_{\pm} from experimental data are plotted in Fig. 2(e), where a clear avoided-crossing behavior is observed and agrees well with the fittings. When the detuning $\Delta = 0$, the minimum of the splitting is $2G$ ($\omega_{\pm} = \omega_{b0} \pm G$) and the spectrum is the sum of two identical Lorentzian shapes with linewidth of $\kappa_{\text{hyb}} = (\kappa_b + \kappa_c)/2$. When $\Delta \neq 0$, Fano-like shapes can be observed in the transmission spectrum as shown in Fig. 2(f). Compared with other nonlinearly coupled systems such as optomechanical [32] and magneto-optical [33] systems, our system has much higher interaction strength G . The cooperativity of our system, however, is currently lower than the

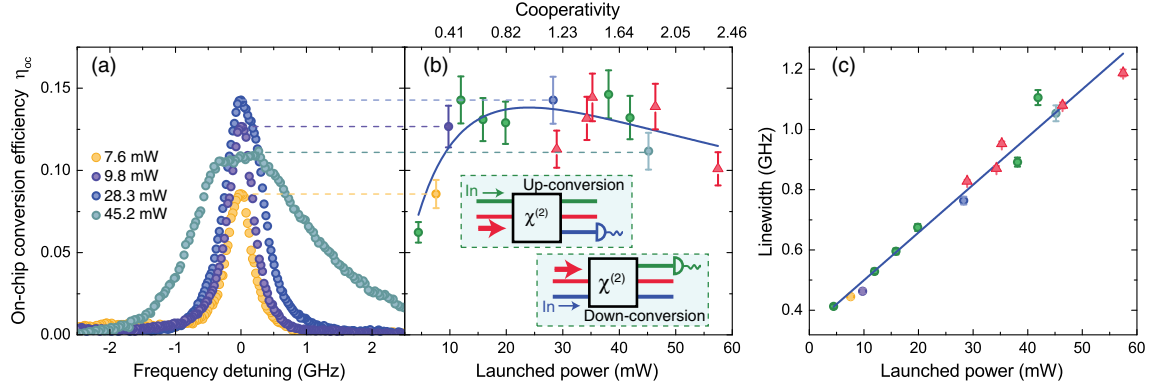


FIG. 3. Optical frequency conversion between the telecom and the visible band. (a) Frequency conversion spectra under different drive laser powers. (b) On-chip conversion efficiency against drive power. The error bar comes from the uncertainty of the fiber-to-chip insertion loss. Triangle data points correspond to frequency down-conversion, while circles correspond to frequency up-conversion. The blue solid line is a fitted curve according to Eq. (6). In both insets, the giant red arrow represents the telecom drive laser. The blue (green) arrow represents seed power of the visible (telecom) probe laser. (c) The linewidth of the frequency conversion spectra under different drive powers.

optomechanical systems [32] due to higher loss rate (on the order of GHz) of our optical modes compared to the low frequency mechanical mode (whose loss rate is on the order of kHz).

While the normal-mode splitting is the hallmark of the coherent interaction, another manifestation of the large coupling between the telecom and visible modes is the high efficiency frequency conversion. From a frequency conversion point of view, the device acts as a beam splitter for different colors of light and the splitting ratio is controlled by the drive laser. As schematically illustrated in the insets of Fig. 3(b), the on-chip conversion efficiency (ratio of photons flux in the output waveguide to the photon flux in the input waveguide) is measured for both up- and down-conversion. The wavelength conversion spectra under different drive laser powers are shown in Fig. 3(a). It is observed that the spectrum is of Lorentzian shape under relatively weak drive power. When the drive laser power is strong enough, the conversion spectrum starts to split. The on-chip conversion efficiency for both up- and down-conversion reads

$$\eta_{oc} = \frac{\kappa_{b,1} \kappa_{c,1}}{\kappa_b \kappa_c} \times \frac{4C}{|(1 + i\frac{\delta_b}{\kappa_b})(1 + i\frac{\delta_c}{\kappa_c}) + C|^2}. \quad (5)$$

For the near-resonance condition that $\delta_c \approx \delta_b \approx 0$,

$$\eta_{oc,max} \approx \frac{\kappa_{b,1} \kappa_{c,1}}{\kappa_b \kappa_c} \times \frac{4C}{|1 + C|^2}. \quad (6)$$

We plot the conversion efficiency against the launched drive laser power as shown in Fig. 3(b). By fitting the experimental results with Eq. (6), we deduce a unit power cooperativity of $0.041 \pm 0.004 \text{ mW}^{-1}$, which agrees well with the value obtained from mode splitting measurement.

According to Eq. (6), the maximum on-chip conversion efficiency will be achieved when $C \approx 1$, which corresponds to a drive laser power around 24.4 mW. Because of nonideal waveguide-to-microring coupling ($\kappa_{c,1}/\kappa_c \approx 0.5$, $\kappa_{b,1}/\kappa_b \approx 0.3$), the achievable on-chip conversion efficiency is limited to be around 0.14. To further increase the on-chip conversion efficiency, both telecom and visible modes need to be overcoupled ($\kappa_{c,1} > \kappa_{c,0}$, $\kappa_{b,1} > \kappa_{b,0}$), while the cooperativity remains as 1. We further study the bandwidth of the frequency conversion under different drive power P_a [Fig. 3(c)]. The nonlinear conversion bandwidth ($\kappa_{cov}/2\pi$) is dependent on the linewidth of both mode b and c , as well as the cooperativity C . We observe a linearly increased conversion bandwidth with increased cooperativity, matching well with the theory that $\kappa_{cov}/2\pi = (1/2\pi)(1 + C)\kappa_b\kappa_c/(\kappa_b + \kappa_c)$. A largest bandwidth of 1.2 GHz is achieved with a drive laser power of 57.5 mW. A unit power cooperativity of $0.046 \pm 0.004 \text{ mW}^{-1}$ is fitted from the data in Fig. 3(c), being consistent with the values extracted from Fig. 2(d) and Fig. 3(b).

The unit power cooperativity is related to the nonlinear single-photon interaction strength g and the linewidth of the optical mode

$$\frac{C}{P_a} = \frac{g^2}{\kappa_a \kappa_b \kappa_c \hbar \omega_a}. \quad (7)$$

By using thick AlN film (1 μm -thick), the waveguide size increases and has better confinement of the optical mode. In addition, we cover the AlN waveguide with SiO_2 top claddings to decrease the refractive index difference and hence the scattering loss. All of these help to reduce the microring radius and increase the quality factors of the optical modes. We also use TM modes to replace TE modes

for higher $\chi^{(2)}$ nonlinearity. These changes lead to a 4 order of magnitude improvement in terms of unit power cooperativity as compared to our previous work [34], making it possible to enter the strong coupling regime. The nonlinear single-photon interaction strength g can be estimated as $g = \sqrt{(C/P_a)\kappa_a\kappa_b\kappa_c\hbar\omega_a} \approx 0.74$ MHz, which is consistent with the theoretically estimated value by assuming $\chi^{(2)} = 1.3$ pm/V [26].

The cooperativity of the system may be further improved. First, in the current experiment the position of the involved optical modes has not been perfectly aligned ($\omega_{a0} + \omega_{c0} - \omega_{b0} \neq 0$). To induce symmetric mode splitting, the drive laser frequency is set to be $\omega_a = \omega_{b0} - \omega_{c0} \neq \omega_{a0}$, which means that the drive laser is detuned from the resonance of mode a and the effective coupling strength G is, hence, reduced. By placing an on-chip heater in the microring, we can finely tune the position of the optical modes through the thermal-optical effect and perfectly fulfill phase match condition ($\omega_{a0} + \omega_{c0} = \omega_{b0}$), leading to higher cooperativity. Second, the single-photon coupling strength g can be improved by reducing mode volume [26]. Third, the quality factor itself can be improved by using even thicker AlN film. Lastly, by applying high peak power driving pulses, the transient driving photon numbers may be improved. For quantum applications, the noise photons from other nonlinear processes need to be carefully addressed. We identify two potential noise sources for our system: Raman scattering and parametric fluorescence generation from spontaneous four wave mixing. Both unwanted processes, however, can be suppressed by selecting the wavelength of the drive laser far away from the coherently coupled telecom and visible modes. We envision the demonstrated strong coupling between two spectrally far-away optical modes renders such device a unique interface for connecting matter qubits at visible wavelength with flying qubits at telecom wavelength, enabling the distributed quantum computation network and quantum communications [23,35].

We thank Liang Jiang for stimulating discussion and Michael Power and Dr. Michael Rooks for assistance in device fabrication. H. X. T. acknowledges support from Defense Advanced Research Projects Agency (DARPA) and the David and Lucile Packard Foundation.

*Corresponding author.
hong.tang@yale.edu

- [1] R. J. Thompson, G. Rempe, and H. J. Kimble, *Phys. Rev. Lett.* **68**, 1132 (1992).
- [2] E. Peter, P. Senellart, D. Martrou, A. Lemaitre, J. Hours, J. M. Gerard, and J. Bloch, *Phys. Rev. Lett.* **95**, 067401 (2005).
- [3] J. Huang and P. Kumar, *Phys. Rev. Lett.* **68**, 2153 (1992).
- [4] M. T. Rakher, L. Ma, O. Slattery, X. Tang, and K. Srinivasan, *Nat. Photonics* **4**, 786 (2010).
- [5] K. De Greve *et al.*, *Nature (London)* **491**, 421 (2012).
- [6] D. V. Strelakov, A. S. Kowligy, Y.-P. Huang, and P. Kumar, *New J. Phys.* **16**, 053025 (2014).
- [7] M. A. Foster, A. C. Turner, J. E. Sharping, B. S. Schmidt, M. Lipson, and A. L. Gaeta, *Nature (London)* **441**, 960 (2006).
- [8] A. H. Gnauck, R. M. Jopson, C. J. McKinstrie, J. C. Centanni, and S. Radic, *Opt. Express* **14**, 8989 (2006).
- [9] I. Agha, M. Davanço, B. Thurston, and K. Srinivasan, *Opt. Lett.* **37**, 2997 (2012).
- [10] C. Dong, V. Fiore, M. C. Kuzyk, and H. Wang, *Science* **338**, 1609 (2012).
- [11] J. T. Hill, A. H. Safavi-Naeini, J. Chan, and O. Painter, *Nat. Commun.* **3**, 1196 (2012).
- [12] D. J. Moss, R. Morandotti, A. L. Gaeta, and M. Lipson, *Nat. Photonics* **7**, 597 (2013).
- [13] B. J. M. Hausmann, I. Bulu, V. Venkataraman, P. Deotare, and M. Lončar, *Nat. Photonics* **8**, 369 (2014).
- [14] D. F. Welch *et al.*, *IEEE J. Sel. Top. Quantum Electron.* **13**, 22 (2007).
- [15] A. Khilo *et al.*, *Opt. Express* **20**, 4454 (2012).
- [16] C. Xiong, W. H. P. Pernice, X. Sun, C. Schuck, K. Y. Fong, and H. X. Tang, *New J. Phys.* **14**, 095014 (2012).
- [17] J. M. Dobrindt, I. Wilson-Rae, and T. J. Kippenberg, *Phys. Rev. Lett.* **101**, 263602 (2008).
- [18] J. Kim, M. C. Kuzyk, K. Han, H. Wang, and G. Bahl, *Nat. Phys.* **11**, 275 (2015).
- [19] C.-H. Dong, Z. Shen, C.-L. Zou, Y.-L. Zhang, W. Fu, and G.-C. Guo, *Nat. Commun.* **6**, 6193 (2015).
- [20] D. Jalas *et al.*, *Nat. Photonics* **7**, 579 (2013).
- [21] L. D. Tzuang, K. Fang, P. Nussenzveig, S. Fan, and M. Lipson, *Nat. Photonics* **8**, 701 (2014).
- [22] Z. Shen, Y.-L. Zhang, Y. Chen, C.-L. Zou, Y.-F. Xiao, X.-B. Zou, F.-W. Sun, G.-C. Guo, and C.-H. Dong, DOI:10.1038/nphoton.2016.161.
- [23] H. J. Kimble, *Nature (London)* **453**, 1023 (2008).
- [24] C. Xiong, W. Pernice, K. K. Ryu, C. Schuck, K. Y. Fong, T. Palacios, and H. X. Tang, *Opt. Express* **19**, 10462 (2011).
- [25] J. S. Levy, M. A. Foster, A. L. Gaeta, and M. Lipson, *Opt. Express* **19**, 11415 (2011).
- [26] See Supplemental Material <http://link.aps.org/supplemental/10.1103/PhysRevLett.117.123902> for theoretical derivation, numerical simulation, and experimental setup, which includes Refs. [27–29].
- [27] L. Fan, J. Wang, L. T. Varghese, H. Shen, B. Niu, Y. Xuan, A. M. Weiner, and M. Qi, *Science* **335**, 447 (2012).
- [28] Y. Shi, Z. Yu, and S. Fan, *Nat. Photonics* **9**, 388 (2015).
- [29] D. F. Walls and G. J. Milburn, *Quantum Optics* (Springer, New York, 2007).
- [30] M. Cai, O. Painter, and K. J. Vahala, *Phys. Rev. Lett.* **85**, 74 (2000).
- [31] S. Weis, R. Rivière, S. Deléglise, E. Gavartin, O. Arcizet, A. Schliesser, and T. J. Kippenberg, *Science* **330**, 1520 (2010).
- [32] S. Gröblacher, K. Hammerer, M. R. Vanner, and M. Aspelmeyer, *Nature (London)* **460**, 724 (2009).
- [33] X. Zhang, N. Zhu, C.-L. Zou, and H. X. Tang, arXiv:1510.03545.
- [34] W. H. P. Pernice, C. Xiong, C. Schuck, and H. X. Tang, *Appl. Phys. Lett.* **100**, 223501 (2012).
- [35] M. G. Raymer and K. Srinivasan, *Phys. Today* **65**, 32 (2012).